Article

Kinetic Stability of $Si_2C_5H_2$ Isomer with a Planar Tetracoordinate Carbon Atom

Krishnan Thirumoorthy [1], Vijayanand Chandrasekaran [1] , Andrew L. Cooksy [2] and Venkatesan S. Thimmakondu [2,*]

[1] School of Advanced Sciences, Vellore Institute of Technology, Vellore 632 014, Tamil Nadu, India; thirumoorthy.krishnan@vit.ac.in (K.T.); vijayanand.c@vit.ac.in (V.C.)
[2] Department of Chemistry and Biochemistry, San Diego State University, San Diego, CA 92182-1030, USA; acooksy@sdsu.edu
* Correspondence: vthimmakondusamy@sdsu.edu

Abstract: Dissociation pathways of the global minimum geometry of $Si_2C_5H_2$ with a planar tetracoordinate carbon (ptC) atom, 2,7-disilatricyclo[$4.1.0.0^{1,3}$]hept-2,4,6-trien-2,7-diyl (**1**), have been theoretically investigated using density functional theory and coupled-cluster (CC) methods. Dissociation of Si-C bond connected to the ptC atom leads to the formation of 4,7-disilabicyclo[4.1.0]hept-1(6),4(5)-dien-2-yn-7-ylidene (**4**) through a single transition state. Dissociation of C-C bond connected to the ptC atom leads to an intermediate with two identical transition states and leads back to **1** itself. Simultaneous breaking of both Si-C and C-C bonds leads to an acyclic transition state, which forms an acyclic product, cis-1,7-disilahept-1,2,3,5,6-pentaen-1,7-diylidene (**19**). Overall, two different products, four transition states, and an intermediate have been identified at the B3LYP/6-311++G(2d,2p) level of theory. Intrinsic reaction coordinate calculations have also been done at the latter level to confirm the isomerization pathways. CC calculations have been done at the CCSD(T)/cc-pVTZ level of theory for all minima. Importantly, all reaction profiles for **1** are found be endothermic in $Si_2C_5H_2$. These results are in stark contrast compared to the structurally similar and isovalent lowest-energy isomer of C_7H_2 with a ptC atom as the overall reaction profiles there have been found to be exothermic. The activation energies for Si-C, C-C, and Si-C/C-C breaking are found to be 30.51, 64.05, and 61.85 kcal mol^{-1}, respectively. Thus, it is emphasized here that **1** is a kinetically stable molecule. However, it remains elusive in the laboratory to date. Therefore, energetic and spectroscopic parameters have been documented here, which may be of relevance to molecular spectroscopists in identifying this key *anti-van't-Hoff-Le Bel* molecule.

Keywords: $Si_2C_5H_2$; planar tetracoordinate carbon; kinetic stability; dissociation pathways; ab initio calculations

1. Introduction

Apart from chemical curiosity, interest in molecules with a planar tetracoordinate [1–8] or hypercoordinate carbon [9–16] atom (ptC or phC) stems from the fact that they could be used as potential new materials [17–21]. Though the experimental evidence on molecules with a ptC atom is limited as of today [22–26], more molecules have been continuously proposed from quantum chemical studies [27–39]. Importantly, two key questions are repeatedly being asked in the synthetic viability of these "*anti-van't Hoff-Le Bel molecules*": [40,41] (i) what is the energetic (thermodynamic) stability of the proposed molecule from a given elemental composition on the molecular potential energy surface (PES)? and (ii) what is its kinetic stability? A firm answer obtained from these two questions either directly or indirectly informs the experimentalists whether the theoretically proposed molecule could possibly be identified in the laboratory or not.

Experimentally, it was outlined in the past that molecules with a ptC atom can be enormously stabilized by the cooperative influence of metal pairs (Zr/Al or Zr/Zr$^+$) of atoms [22]. Experimental confirmation of pentaatomic ptC species (CAl$_4^-$, CAl$_3$Si$^{-/0}$, CAl$_3$Ge$^{-/0}$, CAl$_4^{2-}$, etc.) [23–25] in the gas phase has given the much-needed momentum in the further search of these molecules. Stabilization of ptC by hydrogenation in the case of CAl$_4$H$^{-/0}$ has been observed recently by Bowen and co-workers [26]. The effect of planar tetracoordinate silicon (ptSi) atom [18,33,42–48] in the stability of calix[4]pyrrole hydridosilicate [49] serves as the first experimental proof for ptSi, which motivated further study of these molecules. Very recently, room-temperature stable molecules containing a ptSi atom have been experimentally characterized including single-crystal x-ray diffraction measurements by Filippou and co-workers [50]. In 2017, isomers of X$_2$C$_5$H$_2$ (X = Si, Ge, Sn, and Pb) with a ptC atom have been theoretically proposed as global minimum geometries but to date they are yet to be identified in the laboratory [51]. This indirectly indicates that mere thermodynamic stability is not the only governing factor in the successful identification of molecules in the laboratory [52–57]. Thus, the objective here is to examine the kinetic stability of the global minimum geometry of Si$_2$C$_5$H$_2$ through dissociation studies. The knowledge of activation energies, reaction energies, and the reactive intermediates involved could give sufficient insights to experimentalists in devising successful synthetic routes–including what precursor molecules to choose.

Here, the kinetic stability of 2,7-disilatricyclo[4.1.0.0^{1,3}]hept-2,4,6-trien-2,7-diyl (**1**)—which is the global minimum geometry of Si$_2$C$_5$H$_2$ [51,58]—has been investigated in detail using density functional theory (DFT) and high-level coupled-cluster (CC) methods. Four low-lying isomers of Si$_2$C$_5$H$_2$ including **1** lying within 30 kcal mol^{-1} have been reported at the CCSD(T)/def2-TZVP//PBE0/def2-TZVP level of theory elsewhere [51]. These results were obtained using search algorithms [59–63]. We recently explored the Si$_2$C$_5$H$_2$ PES in an exhaustive manner through a chemical intuition approach [58] instead of using search algorithms. Our study predicted more possible isomers in the low-lying region (see Figure 1). Upon further search, the AUTOMATON program [64], which is based on a genetic algorithm, had also suggested new isomers for Si$_2$C$_5$H$_2$ [58] in the low-lying region. Although the thermodynamic stabilities of various isomers have been examined at length, to the best of our knowledge, the kinetic stability of **1**, which contains a ptC atom, is yet to be studied. Moreover, though it was reported as a global minimum nearly three years ago, the experimental evidence is completely absent not only on **1** but also on all other low-lying Si$_2$C$_5$H$_2$ isomers. Therefore, the kinetic stability of **1** has been examined here, which may possibly aid the detection of this peculiar molecule using infrared or rotational spectroscopy in the laboratory.
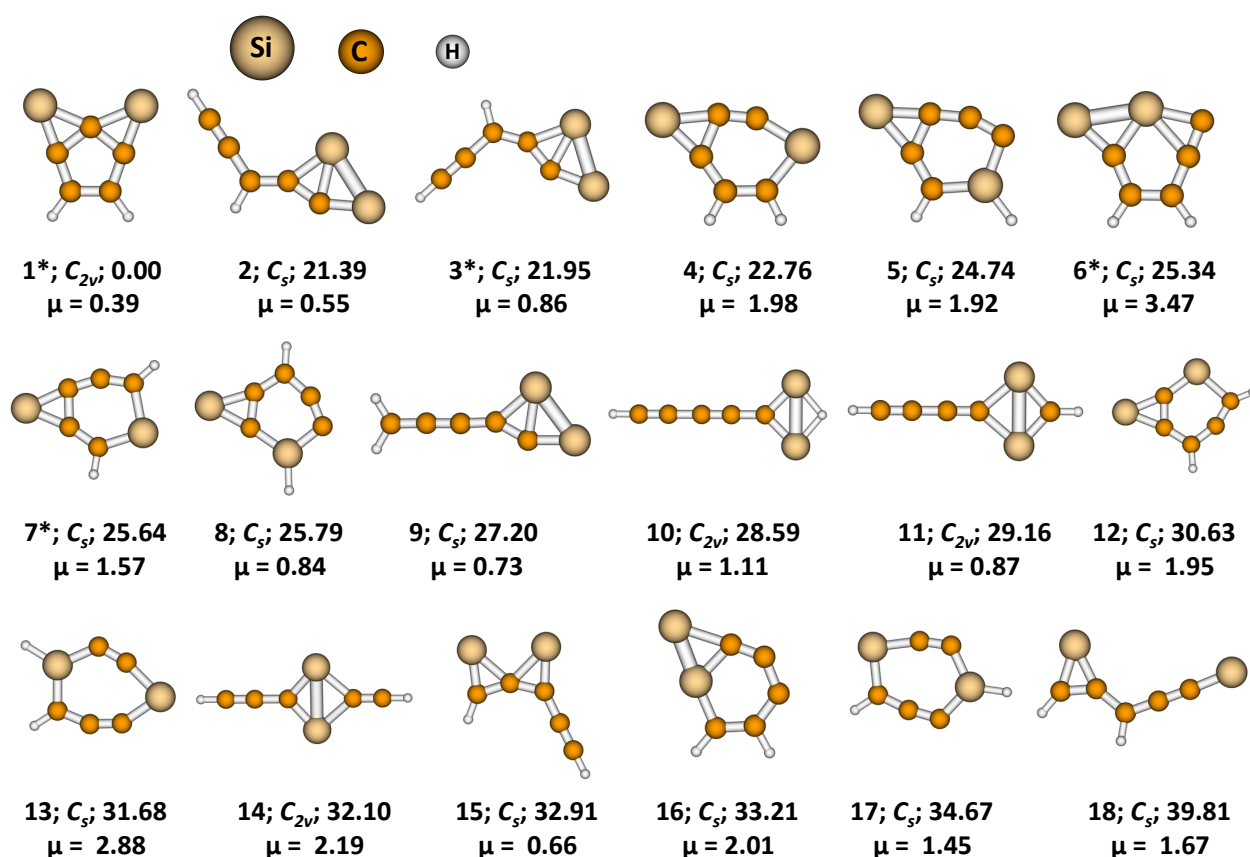
Figure 1. Eighteen low-lying isomers of $Si_2C_5H_2$ currently considered on the singlet PES. Relative energies including ZPVE correction (in kcal mol^{-1}) and dipole moments (in Debye) are calculated at the fc-CCSD(T)/cc-pVTZ level of theory. Isomers identified by search algorithms are marked with an asterisk symbol. All the isomers depicted here are minima and all of them remain elusive in the laboratory to date.

2. Computational Details

The geometries of all $Si_2C_5H_2$ isomers reported here have been optimized using DFT with the B3LYP hybrid-functional [65–68] and the 6-311++G(2d,2p) basis set [69,70]. All the transition states corresponding to the dissociation of C-C/Si-C bonds connected to the ptC atom, the intrinsic reaction coordinate (IRC) calculations [71,72], and the nucleus independent chemical shift (NICS) values [73–75] have been calculated at the latter level. It is also noted here that wavefunction stability analysis has been done for all minima (**1–22**) obtained at the B3LYP/6-311++G(2d,2p) level and no instabilities have been found [76]. All these DFT calculations have been carried out with the Gaussian suite of programs [77]. All the low-lying isomers (minima) obtained from the DFT calculations, which lie within 40 kcal mol^{-1}, have been reoptimized with CC methods. All these CC calculations with single and double excitations (CCSD) [78] including a quasiperturbative triple excitations (CCSD(T)) [79,80] have been done with correlation-consistent polarized valence triple zeta (cc-pVTZ) basis set of Dunning's [81]. The latter basis set consists of 246 basis functions for $Si_2C_5H_2$. The frozen-core (fc) approximation is used for isomers **1–18** initially in the fc-CCSD(T)/cc-pVTZ calculations. For the global minimum geometry alone (**1**), all-electron (ae) calculations at the ae-CCSD(T)/cc-pwCVTZ [82] level of theory have also been done. This basis set consists of 361 basis functions for $Si_2C_5H_2$ and therefore these calculations have not been done for other isomers considering their expensive nature. All these calculations have been done with the CFOUR (2.00 beta version) program package [83]. We note that for all the stationary points obtained, harmonic vibrational frequencies have been calculated by analytic calculation of second derivatives [84].

3. Results and Discussion

Eighteen low-lying isomers of $Si_2C_5H_2$ obtained at the fc-CCSD(T)/cc-pVTZ level of theory are shown in Figure 1. Zero-point vibrational energy (ZPVE) corrected relative energies calculated with respect to **1**, point group symmetry, and the absolute dipole moment value calculated for the corresponding geometry are given underneath each isomer. Optimal geometry parameters obtained at five different levels for isomer **1** are given in Table 1. Harmonic vibrational frequencies, infrared (IR) intensities, and various isotopic shifts (^{28}Si–^{29}Si, ^{12}C–mono-substituted-^{13}C, $Si_2^{13}C_5H_2$, ^1H–mono-substituted-^2D, and $Si_2C_5D_2$) in harmonic vibrational frequencies for isomer **1** are collected in Table 2. The activation energies ($\Delta E^{\ddagger}$), reaction energies (ΔE_r), and relative energies (ΔE_0) calculated at different levels for the various dissociation pathways of **1** are given in Table 3. The atom numbering scheme, natural atomic charges, possible valence structures, and relevant occupied molecular orbitals contributing to the bonding of the ptC atom of isomer **1** are shown in Figure 2. Schematic reaction profile diagram connecting the reactant **1** and their dissociative products through appropriate transition states calculated at the B3LYP/6-311++G(2d,2p) level of theory is shown in Figure 3. Likewise, reaction profile diagram involving the isomerization of **1** to **2** is shown in Figure 4. For brevity, total electronic energies, ZPVEs, and final Cartesian coordinates of the optimized geometries of all isomers are given in the supporting information.
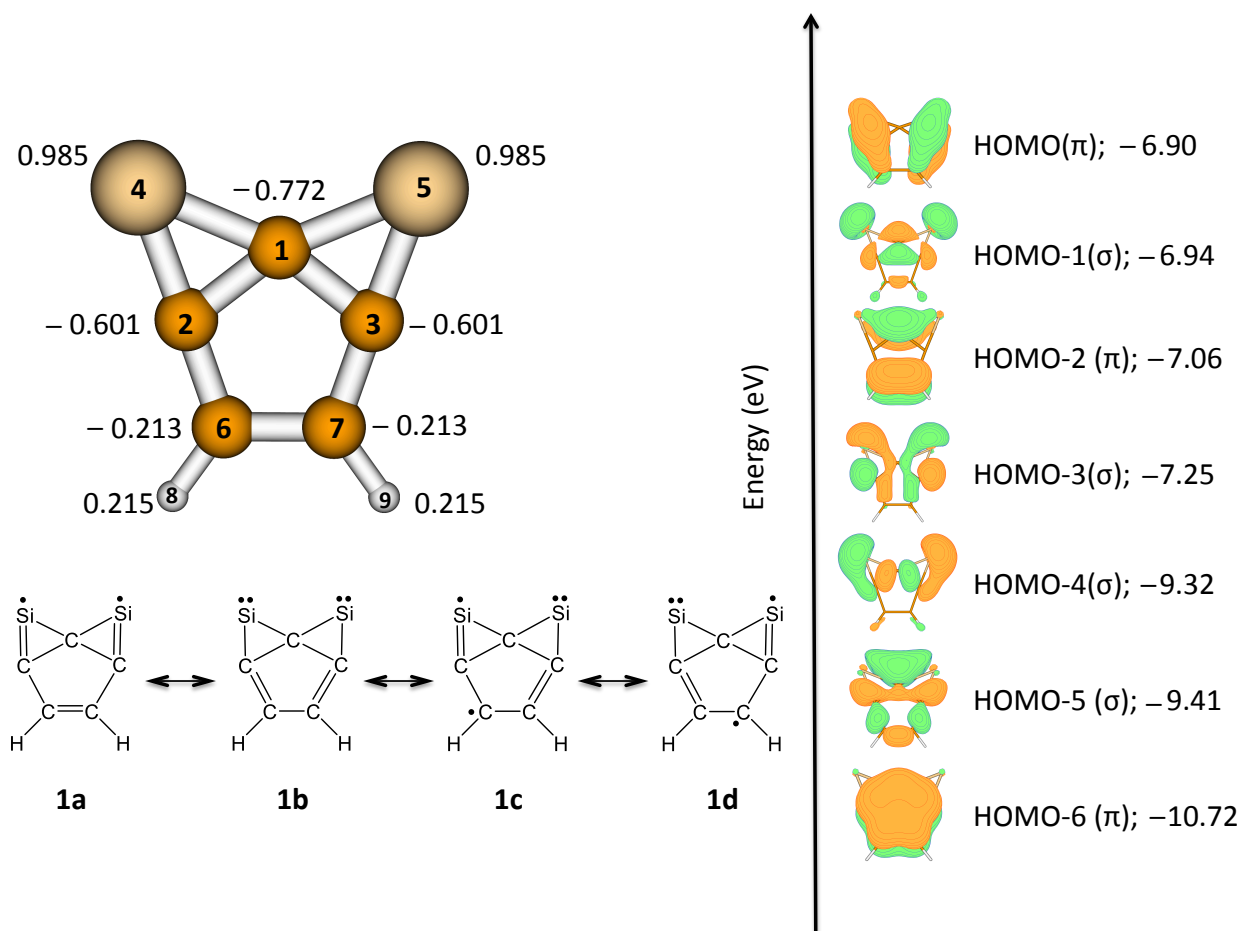

Figure 2. Atom numbering scheme, valence structures, and key occupied molecular orbitals of isomer **1**. Natural atomic charges (in a.u) calculated at the B3LYP/6-311++G(2d,2p) level of theory are also shown.
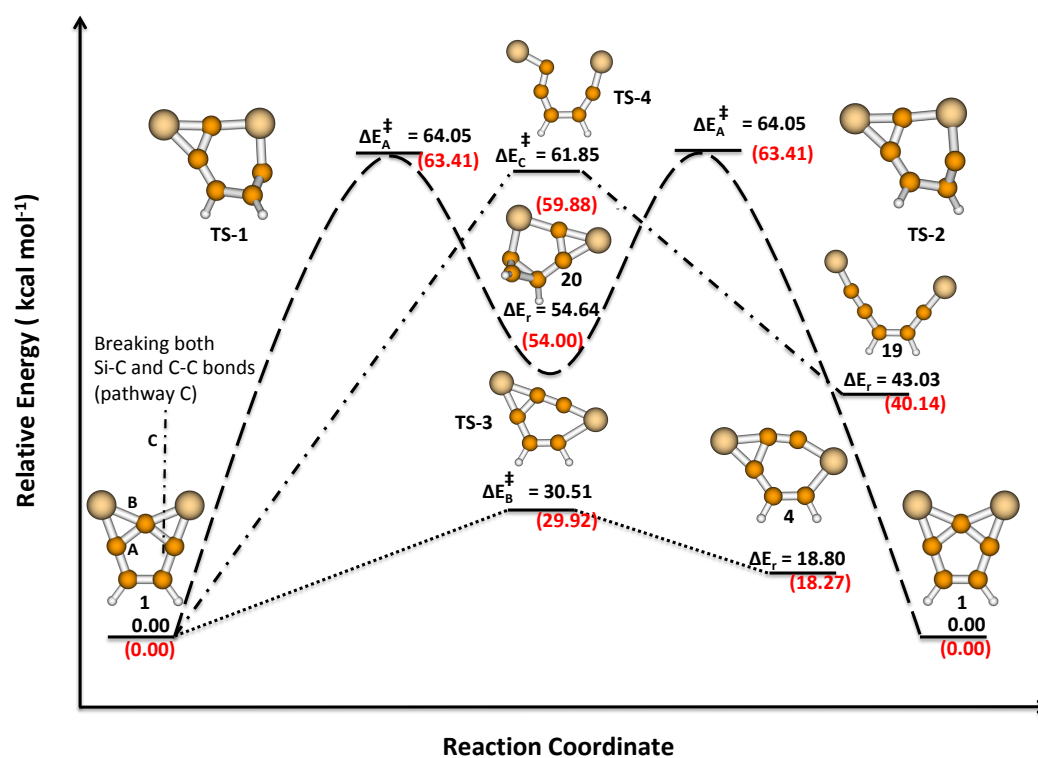
Figure 3. Schematic outline of the dissociation pathways of $Si_2C_5H_2$ global minimum isomer (**1**) with a ptC atom. ZPVE-corrected relative energies are calculated at the B3LYP/6-311++G(2d,2p) level of theory. Gibbs free energy corrected values (at 298.15 K) are given in red color.

Figure 4. Schematic outline of the isomerization pathway of isomer **1** to **2** of $Si_2C_5H_2$. ZPVE-corrected relative energies are calculated at the B3LYP/6-311++G(2d,2p) level of theory. Gibbs free energy corrected values (at 298.15 K) are given in red color. Negative barrier between **21** and **TS-7** is due to ZPVE-corrections. Activation energy (ΔE^*) for the latter route without ZPVE-corrections is 66.96 kcal mol^{-1} (see Section 3.3 for further discussion).

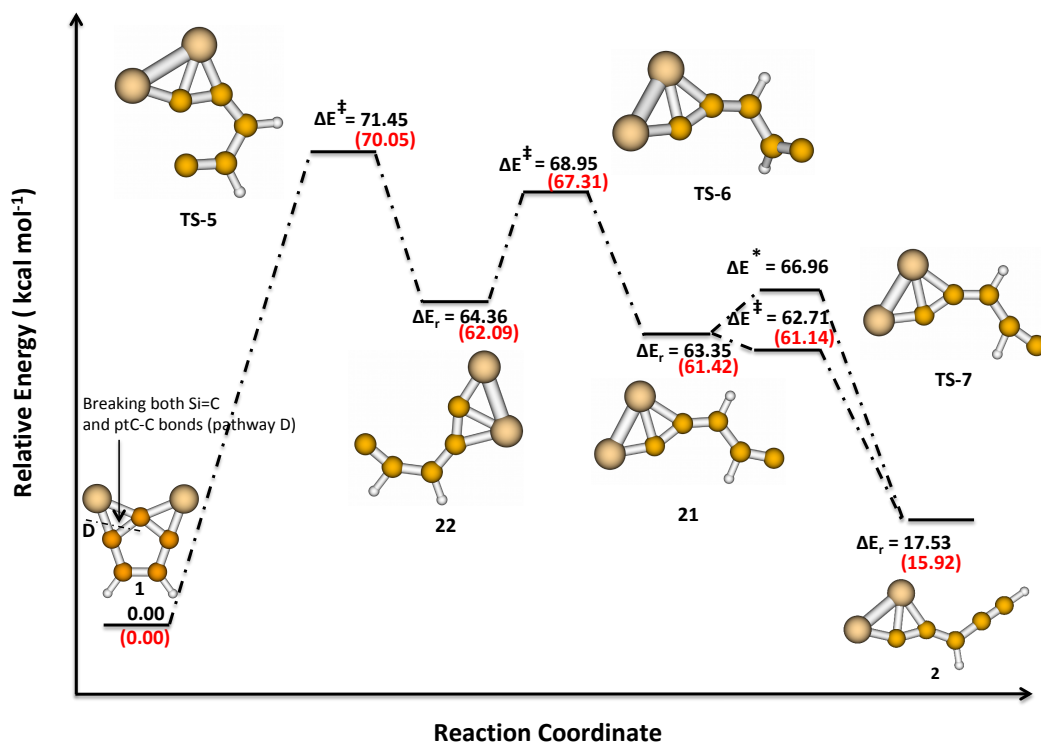**Table 1.** Optimal geometry parameters (Å and degrees) of isomer **1** of $Si_2C_5H_2$ calculated at different levels.

Parameter	B3LYP	CCSD	CCSD(T)	CCSD	CCSD(T)	CCSD(T)
	6-311++G(2d,2p)	cc-pVDZ		cc-pVTZ		cc-pwCVTZ
$R(C_1Si_4;C_1Si_5)$	1.9290	1.9549	1.9612	1.9177	1.9238	1.9081
$R(C_1C_2;C_1C_3)$	1.4679	1.4777	1.4875	1.4677	1.4781	1.4727
$R(C_2Si_4;C_3Si_5)$	1.7506	1.7679	1.7803	1.7488	1.7612	1.7475
$R(C_2C_6;C_3C_7)$	1.4179	1.4379	1.4393	1.4228	1.4244	1.4197
$R(C_6C_7)$	1.3813	1.3914	1.3993	1.3792	1.3876	1.3832
$R(C_6H_8;C_7H_9)$	1.0800	1.0946	1.0968	1.0796	1.0820	1.0806
$\theta(C_2C_1C_3)$	104.00	104.49	104.21	104.44	104.11	104.10
$\theta(C_2C_1Si_4;C_3C_1Si_5)$	60.24	60.10	60.32	60.49	60.69	60.64
$\theta(C_1C_2C_6;C_1C_3C_7)$	108.81	108.57	108.66	108.48	108.60	108.63
$\theta(C_2C_6H_8;C_3C_7H_9)$	124.87	124.82	124.78	124.71	124.67	124.69

Table 2. Harmonic vibrational frequencies, IR Intensities, and isotopic shifts of isomer **1** calculated at the ae-CCSD(T)/cc-pwCVTZ level of theory.

Mode	Isomer 1			Isotopic Shifts (cm^{-1})						
	Symmetry	Frequency	Intensity	^{28}Si–^{29}Si		^{12}C–^{13}C				^{1}H–^{2}D
				Si(4) [a]	^{29}Si$_2$C$_5$H$_2$	C(1)	C(2)	C(6)	Si$_2^{13}$C$_5$H$_2$	H(8)	Si$_2$C$_5$D$_2$
		cm^{-1}	km mol^{-1}								
1	a_2	195.2	0.0	0.4	0.7	0.0	1.9	1.0	5.4	4.3	7.7
2	b_1	219.4	14.7	0.3	0.6	3.9	1.0	0.3	6.6	3.5	8.0
3	a_1	232.8	2.0	1.8	3.6	0.6	0.1	0.1	1.1	0.1	0.3
4	b_2	427.7	106.7	0.7	1.4	3.3	4.0	1.0	12.7	7.9	14.9
5	b_2	513.2	17.8	2.9	5.7	0.6	0.3	2.7	6.6	5.8	9.8
6	a_2	576.7	0.0	0.0	0.0	0.0	5.3	5.0	19.0	37.6	56.1
7	b_1	606.8	0.0	0.0	0.0	10.6	4.7	0.3	22.9	4.4	26.7
8	a_1	616.0	43.6	2.6	5.4	5.3	2.0	1.4	11.5	4.8	11.0
9	a_1	787.9	0.9	0.6	1.1	5.9	5.2	6.9	27.4	85.0	118.1
10	b_1	829.8	20.6	0.0	0.0	0.0	0.5	3.2	7.3	50.6	76.7
11	b_2	887.0	0.1	0.1	0.1	2.9	7.1	8.4	33.0	43.5	125.1
12	a_2	915.7	0.0	0.0	0.0	0.0	0.0	4.6	9.4	33.7	96.6
13	a_1	991.3	30.4	0.0	0.1	16.5	9.2	0.1	36.6	104.1	142.1
14	b_2	1004.5	17.3	0.3	0.7	21.1	0.8	3.5	32.4	9.4	90.5
15	a_1	1103.8	2.3	0.0	0.0	0.1	1.7	3.8	11.2	80.2	99.1
16	b_2	1272.8	13.3	0.4	0.7	2.2	9.3	1.6	19.3	54.5	171.6
17	a_1	1340.0	48.5	0.6	1.2	0.0	17.9	5.6	48.6	9.9	24.1
18	a_1	1461.5	4.2	0.0	0.0	0.0	1.6	24.5	47.2	23.2	45.3
19	b_2	1484.7	8.6	0.3	0.6	0.8	11.1	8.1	49.1	13.5	28.7
20	b_2	3208.9	2.0	0.0	0.0	0.0	0.0	6.4	9.9	825.3	841.2
21	a_1	3227.9	21.1	0.0	0.0	0.0	0.0	4.3	11.4	9.4	828.5

[a] Due to symmetry, Si(4) and Si(5); C(2) and C(3); C(6) and C(7); H(8) and H(9) are equivalent.

Table 3. Dissociation pathways of $Si_2C_5H_2$ isomers (**1** and **2**) and their corresponding activation energies ($\Delta E^{\ddagger}$) and reaction energies (ΔE_r) computed at the B3LYP/6-311++G(2d,2p) level of theory.

Isomer	Dissociation Pathway	$\Delta E^{\ddagger,\,a}$ kcal mol^{-1}	$\Delta E_r{}^{\,b}$ kcal mol^{-1}	$\Delta E_0{}^{\,c}$ kcal mol^{-1}
1	**A**	64.05 (**TS-1;TS-2**)	54.64 (**20**)	0.00
	B	30.51 (**TS-3**)	18.80 (**4**)	22.76
	C	61.85 (**TS-4**)	43.03 (**19**)	$-{}^{\,d}$
	D	71.45 (**TS-5**)	64.36 (**22**)	$-{}^{\,d}$
		68.94 (**TS-6**)	63.35 (**21**)	$-{}^{\,d}$
		62.71 (**TS-7**)	17.53 (**2**)	21.39

^{a} The dissociation pathway leading to the corresponding transition state(s) is (are) given in parenthesis. ^{b} The dissociation pathway leading to the corresponding product is given in parenthesis. The reaction path is confirmed by IRC calculations. ^{c} ZPVE-corrected relative energies of the final product calculated at the fc-CCSD(T)/cc-pVTZ level of theory. In pathway **A**, the final product is **1** and not isomer **20**. ^{d} Not calculated at this level of theory.

3.1. 2,7-Disilatricyclo[4.1.0.0^{1,3}]hept-2,4,6-trien-2,7-diyl (**1**)

All bond lengths of isomer **1** are systematically overestimated at the CCSD/cc-pVDZ and CCSD(T)/cc-pVDZ levels (see Table 1). One could notice a contraction in bond lengths with respect to the same methods using the cc-pVTZ basis set. They are slightly contracted further if we observe the change in bond lengths from CCSD(T)/cc-pVTZ to CCSD(T)/cc-pwCVTZ levels. These results (longer bond lengths with respect to cc-pVDZ basis set) are largely due to the lack of higher angular momentum polarization functions [85–90] and consistent with our earlier observations [91–96]. Considering the double bond characteristics of C_6C_7, C_2Si_4 (C_3Si_5; equal due to C_{2v} symmetry) and single bond characteristics of C_1C_2 (C_1C_3) and C_2C_6 (C_3C_7), we have come to the conclusion that valence structure **1a** shown in Figure 2 is dominant. However, based on the natural atomic charges, one could also assume an equally dominant resonance contributor where the molecule behaves like a zwitterion (Si and H atoms having a partial positive charge whereas all carbon atoms having a partial negative charge). The second most stable isomer, 2-ethynylmethylene-1,4-disilabicyclo[1.1.0]but-1(3)-en-4-ylidene (**2**), is 21.39 kcal mol^{-1} above **1** at the fc-CCSD(T)/cc-pVTZ level of theory (see Figure 1). Therefore, isomer **1** is thermodynamically well-separated from others. It is worth noting here that the singlet-triplet energy gap (ΔE_{ST}) calculated for isomer **1** is 72.26 kcal mol^{-1} (positive value indicates singlet being more stable) at the (U)B3LYP/6-311++G(2d,2p) level of theory [58].

Harmonic vibrational frequencies calculated for **1** reveal that three vibrational modes (modes 4, 8, and 17) are dominant (see Table 2). One is the Si-C-Si rocking (b_2) calculated at 427.7 cm^{-1}, another is the Si-C-Si breathing motion (a_1) calculated at 616.0 cm^{-1}, and yet another is the C-C stretching motion (a_1) calculated at 1340.0 cm^{-1} at the ae-CCSD(T)/cc-pwCVTZ level of theory. Various isotopic shift values calculated by us can help in resolving potential ambiguities in assigning vibrational modes. It is also possible to identify isomer **1** and all other low-lying isomers (**2**–**18**) using Fourier transform microwave spectroscopy as the net dipole moment is non-zero ($\mu \neq 0$) in all cases. The net dipole moment value calculated for isomer **1** is 0.39 Debye at the fc-CCSD(T)/cc-pVTZ level of theory. Rotational and centrifugal distortion constants of all 18 isomers are given in our previous article [58] and detailed discussion related to rotational constants are not repeated here for brevity. It is also noted here that for the low-lying C_7H_2 isomer with a ptC atom, tricyclo[4.1.0.0^{1,3}]hept-2,4,6-trien-2,7-diyl [92], the net dipole moment value calculated at the same level of theory is 5.84 Debye. Such a large deviation is not surprising considering the fact that silicon is more electropositive than carbon and the overall charge (see Figure 2) is more balanced and thus the net dipole moment has a smaller value for isomer **1**. Also, compared with the iso-valent C_7H_2 isomer with a ptC atom, isomer **1** exhibits higher aromatic characteristic. The NICS (1 Å) value obtained for **1** is -20.28 ppm at the B3LYP/6-311++G(2d,2p) level.

At the latter level, the NICS (1 Å) value obtained for C_7H_2 isomer with a ptC atom is −12.21 ppm. Nevertheless, both the molecules remain elusive to date. To analyze the aromatic characteristics further, we have carried out NICS calculations in 3D grid points (see supporting information). The out-of-plane NICS values are negative for all the three rings. On the other hand, the in-plane NICS value (NICS (0 Å)) is positive for the C_5 ring and negative for the SiC_2 rings. Thus, the entire molecule is π-aromatic (see the MOs in Figure 2; HOMO, HOMO-2, HOMO-6) but σ-aromaticity is not completely there in the C_5 ring (HOMO-1, HOMO-3, HOMO-4, HOMO-5). Therefore, isomer **1** of $Si_2C_5H_2$ can be characterized as a molecule, which exhibits pseudo-double aromaticity [97–99]. To assess the multi-reference characteristic of isomer **1**, we have calculated the T_1 diagnostic value suggested elsewhere [100] and found that it is below 0.02. The value obtained for isomer **1** at the fc-CCSD/cc-pVTZ level of theory is 0.015. Thus, we have not carried out multi-reference CC calculations for this molecule.

3.2. Activation and Reaction Energies

To calculate the activation and reaction energies, different bonds connected to the ptC atom of **1** were broken. Four different transition states (**TS-1** to **TS-4**), one intermediate (**20**), and three different products, **1**, 4,7-disilabicyclo[4.1.0]hept-1(6),4(5)-dien-2-yn-7-ylidene (**4**), and cis-1,7-disilahept-1,2,3,5,6-pentaen-1,7-diylidene (**19**), respectively, have been identified (see Figure 3) along three different dissociation pathways **A**, **B**, and **C** connected to the ptC atom of isomer **1**. It is noted here that for pathway **A**, both the reactant and the product are one and the same. Breaking of C-ptC bond requires an $\Delta E^{\ddagger}$ of 64.05 kcal mol^{-1} at the B3LYP/6-311++G(2d,2p) level. IRC calculations through this transition state (**TS-1**) leads to an intermediate (**20**), which lies at 54.64 kcal mol^{-1} above **1**. Another identical transition state, **TS-2**, which is a half-chair equivalent conformer of **TS-1**, has been identified along pathway **A**. IRC calculations along these two transition states (**TS-1** and **TS-2**) either leads to the same non-planar intermediate (**20**—in one direction) or to the global minimum isomer itself (**1**—in the other direction). The lowest activation energy required was estimated to be 30.51 kcal mol^{-1} at the same level of theory, which occurs through Si-ptC bond breaking (pathway **B**). Along pathway **C**, where simultaneous breaking of both C-ptC and Si-ptC bonds has been taken into consideration, an acyclic transition state has been identified (**TS-4**), which requires an activation energy of 61.85 kcal mol^{-1} and leads to an acyclic product, **19**. Overall, the reaction profiles along these three different dissociation pathways are found to be endothermic with a reaction energy of 54.64, 18.80, and 43.03 kcal mol^{-1}, respectively, for dissociation pathways **A**, **B**, and **C**. For the lowest activation energy path (**B**), we have also estimated rate constant values using Rice–Ramsperger–Kassel–Marcus (RRKM) theory [101]. It was estimated that the rate of the reverse reaction (**4** to **1**) is three orders of magnitude faster than the forward reaction. This clearly implies that **1** is kinetically stable.

3.3. Isomerization of **1** to **2**

Isomerization of **1** to **2** has also been considered though **2** lies 21.39 kcal mol^{-1} above **1** (see Figure 4). Considering the structural similarity between **1** and **2**, the Si-C double bond and the ptC-C bonds on one side are initially broken. This requires an activation energy of 71.45 kcal mol^{-1} at the B3LYP/6-311++G(2d,2p) level. IRC calculations from this transition state (**TS-5**) lead us to a new intermediate (**22**). Upon rotating the C-C bond, we found a new transition state (**TS-6**). IRC calculations from **TS-6** lead to new intermediate (**21**), where the hydrogen atoms are in the trans position. A 1,2-H shift must happen to reach the geometry of **2**. Therefore, using this new intermediate **22** and slightly elongating the C-C-C angle, we found a new transition state geometry **TS-7**, which requires an activation energy of 62.71 kcal mol^{-1}. It is noted here that the energy barrier between **21** and **TS-7** is negative after ZPVE-correction at the B3LYP/6-311++G(2d,2p) level. Without ZPVE-corrections, the activation energy (ΔE^*; see Figure 4) is 66.96 kcal mol^{-1}. It is well-known

in the literature that various DFT functionals including the popular B3LYP underestimate the barrier-heights [102,103]. Doubly hybrid density functionals such as B2PLYP [104,105] and XYG3 [102] offer promising alternatives for accurate description of barrier-heights. We leave this discussion with a caveat that currently we have not tried these alternatives and in a future work we would be exploring these avenues. IRC calculations in one direction from **TS-7** lead us to isomer **2**, whose reaction energy is 17.53 kcal mol^{-1}. It is also noted here that the Gibbs free energy change is minimal for almost all stationary points.

3.4. Rate Co-Efficient for the Isomerization Reaction

The activation energies and reaction energies estimated among the low-lying isomers of $Si_2C_5H_2$ reveal that pathway **B** is the most feasible based on energetics. Therefore, for this isomerization process alone, we have calculated the rate coefficients for the forward (k_1) and reverse (k_{-1}) reactions using RRKM theory [101] given by the expression

$$k = N(E - E_{TS})c/\rho \tag{1}$$

where E_{TS} is the energy of the transition state from the ground state of the isomers under consideration, E is the total energy of the isomer, N(E-E_{TS}) is the sum of states of the transition state that would be available for the given energy E of the isomer, c is the velocity of light, and ρ is the density of the vibrational states. The densities of the vibrational states are calculated by Beyer and Swinehart direct count algorithm [106].

The rate of forward and reverse reactions are given in Figure 5 as a function of energy. The reverse reaction is found to be around three orders of magnitude faster than the forward reaction. The equilibrium constant for the isomerization reaction is calculated using the expression K = k_1/k_{-1} and it is given in Figure 6. The equilibrium constant is much below 1. This is due to the high density of vibrational states for isomer **1** (global minimum structure) compared to isomer **4** at energies above the isomerization barrier. This favors the reverse reaction than the forward reaction. Figure 6 clearly indicates that over a wide range of energies, isomer **1** is kinetically as well as energetically more stable.
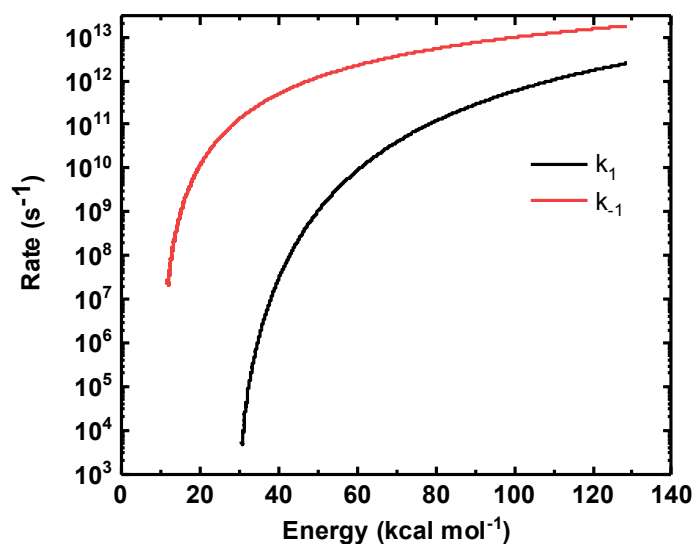

Figure 5. Rate co-efficient for the forward (k_1; **1** to **4**) and reverse (k_{-1}; **4** to **1**) isomerization reaction.
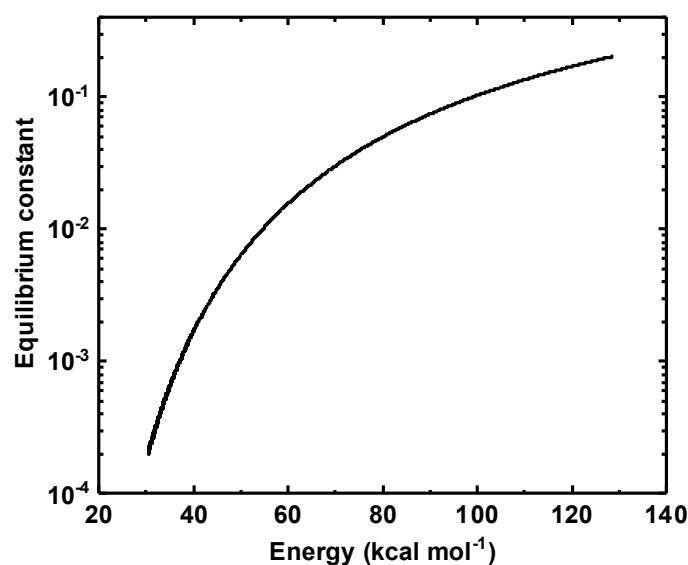
Figure 6. Calculated equilibrium constant for the isomerization reaction of isomers **1** and **4**.

4. Conclusions

The most stable isomer (global minimum) of $Si_2C_5H_2$ containing a ptC atom and its dissociation pathways have been theoretically characterized using DFT and CC methods. The lowest activation energy barrier for **1** has been calculated as 30.51 kcal mol^{-1} at the B3LYP/6-311++G(2d,2p) level of theory. Possible interconversion of **1** to **2** is highly unlikely as the initial activation energy required for this process is 71.45 kcal mol^{-1} at the same level. Hence, it is concluded that **1** is a kinetically stable molecule. Also, the rate co-efficient for the reverse reaction (**4** to **1**; exothermic) is ∼3 orders of magnitude faster than the forward reaction (**1** to **4**; endothermic). This clearly indicates further that isomer **1** is kinetically stable. In fact, our extensive search for various structural isomers of $Si_2C_5H_2$ indicates that there are no other isomers lying close to **1** within 20 kcal mol^{-1} [58] at the fc-CCSD(T)/cc-pVTZ level of theory (see Figure 1). Thus, **1** is not only the energetically most stable molecule but also thermodynamically well-separated from other isomers. Perhaps, synthetic challenges may remain as one of the potential issues in the laboratory identification of this molecule considering the pyrophoric nature of some of the precursor molecules such as SiH_4 in the preparation of this isomer or silicon-doped hydrocarbons, in general. Nevertheless, it is believed that the current theoretical efforts may motivate and assist the experimentalists in devising successful synthetic strategies and in characterizing this potential "*anti-van't Hoff-Le Bel*" molecule in the laboratory. The kinetic stability of 1,7-disilatricyclo[4.1.0.0^{1,3}]hept-2,4,6-trien-2,7-diyl (**6**), which contains a ptSi atom will be examined in a future work.

time provided (to VST) at the National Computational Infrastructure (NCI), which is supported by the Australian Government, is also gratefully acknowledged.

Institutional Review Board Statement: Not applicable.

Informed Consent Statement: Not applicable.

Data Availability Statement: The data presented in this study are available in inside the article or the supplementary material.

Abbreviations

The following abbreviations are used in this manuscript:

ae	all-electron
fc	frozen-core
DFT	Density functional theory
CCSD	Coupled-cluster singles, doubles
CCSD(T)	Coupled-cluster singles, doubles including perturbative triples
ptC	planar tetracoordinate carbon
ptSi	planar tetracoordinate silicon

References

1. Hoffmann, R.; Alder, R.W.; Wilcox, C.F. Planar Tetracoordinate Carbon. *J. Am. Chem. Soc.* **1970**, *92*, 4992–4993. [CrossRef]
2. Collins, J.B.; Dill, J.D.; Jemmis, E.D.; Apeloig, Y.; Schleyer, P.V.R.; Seeger, R.; Pople, J.A. Stabilization of Planar Tetracoordinate Carbon. *J. Am. Chem. Soc.* **1976**, *98*, 5419–5427. [CrossRef]
3. Keese, R. Carbon Flatland: Planar Tetracoordinate Carbon and Fenestranes. *Chem. Rev.* **2006**, *106*, 4787–4808. [CrossRef] [PubMed]
4. Radom, L.; Rasmussen, D.R. The Planar Carbon Story. *Pure Appl. Chem.* **1998**, *70*, 1977. [CrossRef]
5. Merino, G.; Méndez-Rojas, M.A.; Beltrán, H.I.; Corminboeuf, C.; Heine, T.; Vela, A. Theoretical Analysis of the Smallest Carbon Cluster Containing a Planar Tetracoordinate Carbon. *J. Am. Chem. Soc.* **2004**, *126*, 16160–16169. [CrossRef]
6. Pancharatna, P.D.; Méndez-Rojas, M.A.; Merino, G.; Vela, A.; Hoffmann, R. Planar Tetracoordinate Carbon in Extended Systems. *J. Am. Chem. Soc.* **2004**, *126*, 15309–15315. [CrossRef]
7. Roy, D.; Corminboeuf, C.; Wannere, C.S.; King, R.B.; Schleyer, P.V.R. Planar Tetracoordinate Carbon Atoms Centered in Bare Four-membered Rings of Late Transition Metals. *Inorg. Chem.* **2006**, *45*, 8902–8906. [CrossRef]
8. Nandula, A.; Trinh, Q.T.; Saeys, M.; Alexandrova, A.N. Origin of Extraordinary Stability of Square-Planar Carbon Atoms in Surface Carbides of Cobalt and Nickel. *Angew. Chem. Int. Ed.* **2015**, *54*, 5312–5316. [CrossRef]
9. Yang, L.M.; Ganz, E.; Chen, Z.; Wang, Z.X.; Schleyer, P.v.R. Four Decades of the Chemistry of Planar Hypercoordinate Compounds. *Angew. Chem. Int. Ed.* **2015**, *54*, 9468–9501. [CrossRef]
10. Yañez, O.; Báez-Grez, R.; Garza, J.; Pan, S.; Barroso, J.; Vásquez-Espinal, A.; Merino, G.; Tiznado, W. Embedding a Planar Hypercoordinate Carbon Atom into a [4n+2] π-System. *ChemPhysChem* **2020**, *21*, 145–148. [CrossRef]
11. Guo, J.C.; Feng, L.Y.; Dong, C.; Zhai, H.J. Planar Pentacoordinate versus Tetracoordinate Carbons in Ternary CBe_4Li_4 and $CBe_4Li_4^{2-}$ Clusters. *J. Phys. Chem. A* **2018**, *122*, 8370–8376. [CrossRef] [PubMed]
12. Zhang, C.F.; Han, S.J.; Wu, Y.B.; Lu, H.G.; Lu, G. Thermodynamic Stability versus Kinetic Stability: Is the Planar Hexacoordinate Carbon Species D_{3h} $CN_3Mg_3^+$ Viable? *J. Phys. Chem. A* **2014**, *118*, 3319–3325. [CrossRef] [PubMed]
13. Wu, Y.B.; Duan, Y.; Lu, H.G.; Li, S.D. $CAl_2Be_3^{2-}$ and Its Salt Complex $LiCAl_2Be_3^-$: Anionic Global Minima with Planar Pentacoordinate Carbon. *J. Phys. Chem. A* **2012**, *116*, 3290–3294. [CrossRef] [PubMed]
14. Guo, J.C.; Feng, L.Y.; Zhang, X.Y.; Zhai, H.J. Star-Like $CBe_5Au_5^+$ Cluster: Planar Pentacoordinate Carbon, Superalkali Cation, and Multifold (π and σ) Aromaticity. *J. Phys. Chem. A* **2018**, *122*, 1138–1145. [CrossRef]
15. Wang, M.H.; Dong, X.; Ding, Y.H.; Cui, Z.H. Avoided Spin Coupling: An Unexpected σ-σ Diradical in Global Planar Pentacoordinate Carbon. *Chem. Commun.* **2020**, *56*, 7285–7288. [CrossRef]
16. Guo, J.C.; Feng, L.Y.; Barroso, J.; Merino, G.; Zhai, H.J. Planar or Tetrahedral? A Ternary 17-Electron $CBe_5H_4^+$ Cluster with Planar Pentacoordinate Carbon. *Chem. Commun.* **2020**, *56*, 8305–8308. [CrossRef]
17. Wang, Y.; Li, F.; Li, Y.; Chen, Z. Semi-Metallic Be_5C_2 Monolayer Global Minimum with Quasi-Planar Pentacoordinate Carbons and Negative Poisson's Ratio. *Nat. Commun.* **2016**, *7*, 11488. [CrossRef]

18. Li, Y.; Li, F.; Zhou, Z.; Chen, Z. SiC$_2$ Silagraphene and Its One-Dimensional Derivatives: Where Planar Tetracoordinate Silicon Happens. *J. Am. Chem. Soc.* **2011**, *133*, 900–908. [CrossRef]

19. Wang, M.H.; Dong, X.; Cui, Z.H.; Orozco-Ic, M.; Ding, Y.H.; Barroso, J.; Merino, G. Planar Pentacoordinate Silicon and Germanium Atoms. *Chem. Commun.* **2020**, *56*, 13772–13775. [CrossRef]

20. Jimenez-Izal, E.; Saeys, M.; Alexandrova, A.N. Metallic and Magnetic 2D Materials Containing Planar Tetracoordinated C and N. *J. Phys. Chem. C* **2016**, *120*, 21685–21690. [CrossRef]

21. Zhang, C.; Tian, Z.; Jia, W.; Mo, Y. Rational Design of Porous Organic Molecules (POMs) Based on B-Heterocyclic Carbenes. *Mol. Syst. Des. Eng.* **2021**, doi:10.1039/D0ME00156B. [CrossRef]

22. Röttger, D.; Erker, G. Compounds Containing Planar-Tetracoordinate Carbon. *Angew. Chem. Int. Ed. Engl.* **1997**, *36*, 812–827. [CrossRef]

23. Li, X.; Wang, L.S.; Boldyrev, A.I.; Simons, J. Tetracoordinated Planar Carbon in the Al$_4$C$^-$ Anion. A Combined Photoelectron Spectroscopy and ab Initio Study. *J. Am. Chem. Soc.* **1999**, *121*, 6033–6038. [CrossRef]

24. Wang, L.S.; Boldyrev, A.I.; Li, X.; Simons, J. Experimental Observation of Pentaatomic Tetracoordinate Planar Carbon-Containing Molecules. *J. Am. Chem. Soc.* **2000**, *122*, 7681–7687. [CrossRef]

25. Li, X.; Zhang, H.F.; Wang, L.S.; Geske, G.; Boldyrev, A. Pentaatomic Tetracoordinate Planar Carbon, [CAl$_4$]$^{2-}$: A New Structural Unit and Its Salt Complexes. *Angew. Chem. Int. Ed.* **2000**, *39*, 3630–3632. [CrossRef]

26. Xu, J.; Zhang, X.; Yu, S.; Ding, Y.H.; Bowen, K.H. Identifying the Hydrogenated Planar Tetracoordinate Carbon: A Combined Experimental and Theoretical Study of CAl$_4$H and CAl$_4$H$^-$. *J. Phys. Chem. Lett.* **2017**, *8*, 2263–2267. [CrossRef]

27. Priyakumar, U.D.; Reddy, A.S.; Sastry, G.N. The Design of Molecules Containing Planar Tetracoordinate Carbon. *Tetrahedron Lett.* **2004**, *45*, 2495–2498. [CrossRef]

28. Perez, N.; Heine, T.; Barthel, R.; Seifert, G.; Vela, A.; Mendez-Rojas, M.A.; Merino, G. Planar Tetracoordinate Carbons in Cyclic Hydrocarbons. *Org. Lett.* **2005**, *7*, 1509–1512. [CrossRef]

29. Sateesh, B.; Srinivas Reddy, A.; Narahari Sastry, G. Towards Design of the Smallest Planar Tetracoordinate Carbon and Boron Systems. *J. Comput. Chem.* **2007**, *28*, 335–343. [CrossRef]

30. Cui, Z.H.; Ding, Y.H.; Cabellos, J.L.; Osorio, E.; Islas, R.; Restrepo, A.; Merino, G. Planar Tetracoordinate Carbons with A Double Bond in CAl$_3$E Clusters. *Phys. Chem. Chem. Phys.* **2015**, *17*, 8769–8775. [CrossRef]

31. Suresh, C.H.; Frenking, G. Direct 1-3 Metal-Carbon Bonding and Planar Tetracoordinated Carbon in Group 6 Metallacyclobutadienes. *Organometallics* **2010**, *29*, 4766–4769. [CrossRef]

32. Cui, Z.H.; Contreras, M.; Ding, Y.H.; Merino, G. Planar Tetracoordinate Carbon versus Planar Tetracoordinate Boron: The Case of CB$_4$ and Its Cation. *J. Am. Chem. Soc.* **2011**, *133*, 13228–13231. [CrossRef] [PubMed]

33. Thimmakondu, V.S.; Thirumoorthy, K. Si$_3$C$_2$H$_2$ Isomers with A Planar Tetracoordinate Carbon or Silicon atom(s). *Comput. Theor. Chem.* **2019**, *1157*, 40–46. [CrossRef]

34. Thirumoorthy, K.; Karton, A.; Thimmakondu, V.S. From High-Energy C$_7$H$_2$ Isomers with A Planar Tetracoordinate Carbon Atom to An Experimentally Known Carbene. *J. Phys. Chem. A* **2018**, *122*, 9054–9064. [CrossRef] [PubMed]

35. Thirumoorthy, K.; Thimmakondu, V.S. Flat Crown Ethers with Planar Tetracoordinate Carbon Atoms. *Int. J. Quantum Chem.* **2020**, e26479. [CrossRef]

36. Raghunathan, S.; Yadav, K.; Rojisha, V.C.; Jaganade, T.; Prathyusha, V.; Bikkina, S.; Lourderaj, U.; Priyakumar, U.D. Transition Between [R]- and [S]-Stereoisomers without Bond Breaking. *Phys. Chem. Chem. Phys.* **2020**, *22*, 14983–14991. [CrossRef]

37. Job, N.; Karton, A.; Thirumoorthy, K.; Cooksy, A.L.; Thimmakondu, V.S. Theoretical Studies of SiC$_4$H$_2$ Isomers Delineate Three Low-Lying Silylidenes Are Missing in the Laboratory. *J. Phys. Chem. A* **2020**, *124*, 987–1002. [CrossRef]

38. Zhang, C.; Wang, P.; Liang, J.; Jia, W.; Cao, Z. Theoretical Study on a Family of Organic Molecules with Planar Tetracoordinate Carbon. *J. Mol. Struct. THEOCHEM* **2010**, *941*, 41–46. [CrossRef]

39. Yañez, O.; Vásquez-Espinal, A.; Báez-Grez, R.; Rabanal-León, W.A.; Osorio, E.; Ruiz, L.; Tiznado, W. Carbon Rings Decorated with Group 14 Elements: New Aromatic Clusters Containing Planar Tetracoordinate Carbon. *New J. Chem.* **2019**, *43*, 6781–6785.

40. Van't Hoff, J.H. A Suggestion Looking to the Extension Into Space of the Structural Formulas at Present Used in Chemistry. And A Note Upon the Relation Between the Optical Activity and the Chemical Constitution of Organic Compounds. *Arch. Neerl. Sci. Exactes Nat.* **1874**, *9*, 445–454.

41. Le-Bel, J.A. On the Relations Which Exist Between the Atomic Formulas of Organic Compounds and the Rotatory Power of Their Solutions. *Bull. Soc. Chim. Fr.* **1874**, *22*, 337–347.

42. Würthwein, E.U.; von Ragué Schleyer, P. Planar Tetracoordinate Silicon. *Angew. Chem. Int. Ed. Engl.* **1979**, *18*, 553–554. [CrossRef]

43. Guo, J.C.; Miao, C.Q.; Ren, G.M. Planar Tetracoordinate Si and Ge in π-Aromatic X$_3$Cu$_3^+$ (X=Si, Ge) Cations. *Comput. Theor. Chem.* **2014**, *1032*, 7–11. [CrossRef]

44. Guo, J.C.; Wu, H.X.; Ren, G.M.; Miao, C.Q.; Li, Y.X. D_{3h} X$_3$Li$_3^+$ (X=C, Si and Ge): Superalkali Cations Containing Three Planar Tetracoordinate X Atoms. *Comput. Theor. Chem.* **2016**, *1083*, 1–6. [CrossRef]

45. Li, S.D.; Miao, C.Q.; Guo, J.C.; Ren, G.M. Planar Tetra-, Penta-, Hexa-, Hepta-, and Octacoordinate Silicons: A Universal Structural Pattern. *J. Am. Chem. Soc.* **2004**, *126*, 16227–16231. [CrossRef]

46. Sui, J.J.; Xu, J.; Ding, Y.H. A Template for A Planar Tetracoordinate Heavier Group 14 Atom: A Global Study of C$_2$Si$_2$X^q (X = C, Si, Ge, Sn, Pb; q = +1, 0, −1). *Dalton Trans.* **2016**, *45*, 56–60. [CrossRef]

47. Xu, J.; Ding, Y.H. Pentaatomic Planar Tetracoordinate Silicon with 14 Valence Electrons: A Large-Scale Global Search of $SiX_nY_q^m$ (n + m = 4; q = 0, ±1, −2; X, Y = Main Group Elements From H to Br). *J. Comput. Chem.* **2015**, *36*, 355–360. [CrossRef]

48. Zhang, Y.; Zhang, C.; Mo, Y.; Cao, Z. Planar Tetracoordinate Silicon in Organic Molecules As Carbenoid-Type Amphoteric Centers: A Computational Study. *Chem. Eur. J.* **2020**, *26*, 1–9. doi:10.1002/chem.202004298. [CrossRef]

49. Ebner, F.; Greb, L. Calix[4]pyrrole Hydridosilicate: The Elusive Planar Tetracoordinate Silicon Imparts Striking Stability to Its Anionic Silicon Hydride. *J. Am. Chem. Soc.* **2018**, *140*, 17409–17412. [CrossRef]

50. Ghana, P.; Rump, J.; Schnakenburg, G.; Arz, M.I.; Filippou, A.C. Planar Tetracoordinated Silicon (ptSi): Room-Temperature Stable Compounds Containing Anti-van't Hoff/Le Bel Silicon. *J. Am. Chem. Soc.* **2020**, doi:10.1021/jacs.0c11628. [CrossRef]

51. Yañez, O.; Vásquez-Espinal, A.; Pino-Rios, R.; Ferraro, F.; Pan, S.; Osorio, E.; Merino, G.; Tiznado, W. Exploiting Electronic Strategies to Stabilize A Planar Tetracoordinate Carbon in Cyclic Aromatic Hydrocarbons. *Chem. Commun.* **2017**, *53*, 12112–12115. [CrossRef] [PubMed]

52. Reusch, E.; Kaiser, D.; Schleier, D.; Buschmann, R.; Krueger, A.; Hermann, T.; Engels, B.; Fischer, I.; Hemberger, P. Pentadiynylidene and Its Methyl-Substituted Derivates: Threshold Photoelectron Spectroscopy of R_1-C_5-R_2 Triplet Carbon Chains. *J. Phys. Chem. A* **2019**, *123*, 2008–2017. [CrossRef] [PubMed]

53. Bouwman, J.; Bodi, A.; Hemberger, P. Nitrogen Matters: The Difference Between PANH and PAH Formation. *Phys. Chem. Chem. Phys.* **2018**, *20*, 29910–29917. [CrossRef] [PubMed]

54. Henkel, S.; Huynh, Y.A.; Neuhaus, P.; Winkler, M.; Sander, W. Tunneling Rearrangement of 1-Azulenylcarbene. *J. Am. Chem. Soc.* **2012**, *134*, 13204–13207. [CrossRef]

55. Fulara, J.; Nagy, A.; Filipkowski, K.; Thimmakondu, V.S.; Stanton, J.F.; Maier, J.P. Electronic Transitions of $C_6H_4^+$ Isomers: Neon Matrix and Theoretical Studies. *J. Phys. Chem. A* **2013**, *117*, 13605–13615. [CrossRef]

56. Thimmakondu, V.S. MgC_2H_2 isomers—Simple Penta-Atomic Molecules Missing in the Laboratory. *Chem. Phys.* **2020**, *538*, 110899. [CrossRef]

57. Pandey, A.P.; Padidela, U.K.; Thulasiraman, L.K.; Sethu, R.; Vairaprakash, P.; Thimmakondu, V.S. MgC_6H_2 Isomers: Potential Candidates for Laboratory and Radioastronomical Studies. *J. Phys. Chem. A* **2020**, *124*, 7518–7525. [CrossRef]

58. Thirumoorthy, K.; Cooksy, A.; Thimmakondu, V.S. $Si_2C_5H_2$ Isomers—Search Algorithms Versus Chemical Intuition. *Phys. Chem. Chem. Phys.* **2020**, *22*, 5865–5872. [CrossRef]

59. Saunders, M. Stochastic Search for Isomers on a Quantum Mechanical Surface. *J. Comput. Chem.* **2004**, *25*, 621–626. [CrossRef]

60. Bera, P.P.; Sattelmeyer, K.W.; Saunders, M.; Schaefer, H.F.; Schleyer, P.V.R. Mindless Chemistry. *J. Phys. Chem. A* **2006**, *110*, 4287–4290. [CrossRef]

61. Zhao, J.; Xie, R.H. Genetic Algorithms for the Geometry Optimization of Atomic and Molecular Clusters. *J. Comput. Theor. Nanosci.* **2004**, *1*, 117–131. [CrossRef]

62. Grande-Aztatzi, R.; Martínez-Alanis, P.R.; Cabellos, J.L.; Osorio, E.; Martínez, A.; Merino, G. Structural Evolution of Small Gold Clusters Doped by One and Two Boron Atoms. *J. Comput. Chem.* **2014**, *35*, 2288–2296. [CrossRef] [PubMed]

63. Ramirez-Manzanares, A.; Peña, J.; Azpiroz, J.M.; Merino, G. A Hierarchical Algorithm for Molecular Similarity (H-FORMS). *J. Comput. Chem.* **2015**, *36*, 1456–1466. [CrossRef] [PubMed]

64. Yañez, O.; Báez-Grez, R.; Inostroza, D.; Rabanal-León, W.A.; Pino-Rios, R.; Garza, J.; Tiznado, W. AUTOMATON: A Program That Combines a Probabilistic Cellular Automata and a Genetic Algorithm for Global Minimum Search of Clusters and Molecules. *J. Chem. Theory Comput.* **2019**, *15*, 1463–1475.

65. Lee, C.; Yang, W.; Parr, R.G. Development of the Colle-Salvetti correlation-energy formula into a functional of the electron density. *Phys. Rev. B* **1988**, *37*, 785–789. [CrossRef]

66. Becke, A.D. Density-Functional Exchange-Energy Approximation with Correct Asymptotic Behavior. *Phys. Rev. A* **1988**, *38*, 3098–3100. [CrossRef]

67. Becke, A.D. Density-Functional Thermochemistry. III. The Role of Exact Exchange. *J. Chem. Phys.* **1993**, *98*, 5648–5652. [CrossRef]

68. Stephens, P.J.; Devlin, F.J.; Chabalowski, C.F.; Frisch, M. Ab Initio Calculation of Vibrational Absorption and Circular Dichroism Spectra Using Density Functional Force Fields. *J. Phys. Chem.* **1994**, *98*, 11623–11627. [CrossRef]

69. Krishnan, R.; Binkley, J.S.; Seeger, R.; Pople, J.A. Self-Consistent Molecular Orbital Methods. XX. A Basis Set for Correlated Wave Functions. *J. Chem. Phys.* **1980**, *72*, 650–654. [CrossRef]

70. Clark, T.; Chandrasekhar, J.; Spitznagel, G.W.; Schleyer, P.V.R. Efficient Diffuse Function-Augmented Basis Sets for Anion Calculations. III. The 3-21+G Basis Set for First-Row Elements, Li-F. *J. Comput. Chem.* **1983**, *4*, 294–301. [CrossRef]

71. Fukui, K. The Path of Chemical Reactions—The IRC Approach. *Acc. Chem. Res.* **1981**, *14*, 363–368. [CrossRef]

72. Hratchian, H.P.; Schlegel, H.B. Chapter 10—Finding Minima, Transition States, and Following Reaction Pathways On Ab Initio Potential Energy Surfaces. In *Theory and Applications of Computational Chemistry*; Dykstra, C.E., Frenking, G., Kim, K.S., Scuseria, G.E., Eds.; Elsevier: Amsterdam, The Netherlands, 2005; pp. 195–249.

73. Chen, Z.; Wannere, C.S.; Corminboeuf, C.; Puchta, R.; Schleyer, P.V.R. Nucleus-Independent Chemical Shifts (NICS) as an Aromaticity Criterion. *Chem. Rev.* **2005**, *105*, 3842–3888. [CrossRef] [PubMed]

74. Fallah-Bagher-Shaidaei, H.; Wannere, C.S.; Corminboeuf, C.; Puchta, R.; Schleyer, P.V.R. Which NICS Aromaticity Index for Planar π Rings Is Best? *Org. Lett.* **2006**, *8*, 863–866. [CrossRef] [PubMed]

75. Seal, P.; Chakrabarti, S. Is Nucleus-Independent Chemical Shift Scan a Reliable Aromaticity Index for Planar Heteroatomic Ring Systems? *J. Phys. Chem. A* **2007**, *111*, 9988–9994. [CrossRef]

76. Bauernschmitt, R.; Ahlrichs, R. Stability Analysis for Solutions of the Closed Shell Kohn–Sham Equation. *J. Chem. Phys.* **1996**, *104*, 9047–9052. [CrossRef]

77. Frisch, M.J.; Trucks, G.W.; Schlegel, H.B.; Scuseria, G.E.; Robb, M.A.; Cheeseman, J.R.; Scalmani, G.; Barone, V.; Petersson, G.A.; Nakatsuji, H.; et al. *Gaussian 16 Revision B.01*; Gaussian Inc.: Wallingford, CT, USA, 2016.

78. Purvis, G.D.; Bartlett, R.J. A Full Coupled-Cluster Singles and Doubles Model: The Inclusion of Disconnected Triples. *J. Chem. Phys.* **1982**, *76*, 1910–1918. [CrossRef]

79. Raghavachari, K.; Trucks, G.W.; Pople, J.A.; Head-Gordon, M. A Fifth-Order Perturbation Comparison of Electron Correlation Theories. *Chem. Phys. Lett.* **1989**, *157*, 479–483. [CrossRef]

80. Bartlett, R.J.; Watts, J.; Kucharski, S.; Noga, J. Non-Iterative Fifth-Order Triple and Quadruple Excitation Energy Corrections in Correlated Methods. *Chem. Phys. Lett.* **1990**, *165*, 513–522. [CrossRef]

81. Dunning, T.H. Gaussian Basis Sets for Use In Correlated Molecular Calculations. I. The Atoms Boron Through Neon and Hydrogen. *J. Chem. Phys.* **1989**, *90*, 1007–1023. [CrossRef]

82. Peterson, K.A.; Dunning, T.H. Accurate Correlation Consistent Basis Sets for Molecular Core–Valence Correlation Effects: The Second Row Atoms Al-Ar, and the First Row Atoms B-Ne Revisited. *J. Chem. Phys.* **2002**, *117*, 10548–10560. [CrossRef]

83. Stanton, J.F.; Gauss, J.; Cheng, L.; Harding, M.E.; Matthews, D.A.; Szalay, P.G. CFOUR, Coupled-Cluster Techniques for Computational Chemistry, a Quantum-Chemical Program Package. With Contributions from A.A. Auer, R.J. Bartlett, U. Benedikt, C. Berger, D.E. Bernholdt, Y.J. Bomble, O. Christiansen, F. Engel, R. Faber, M. Heckert, O. Heun, M. Hilgenberg, C. Huber, T.-C. Jagau, D. Jonsson, J. Jusélius, T. Kirsch, K. Klein, W.J. Lauderdale, F. Lipparini, T. Metzroth, L.A. Mück, D.P. O'Neill, D.R. Price, E. Prochnow, C. Puzzarini, K. Ruud, F. Schiffmann, W. Schwalbach, C. Simmons, S. Stopkowicz, A. Tajti, J. Vázquez, F. Wang, J.D. Watts and the integral packages MOLECULE (J. Almlöf and P.R. Taylor), PROPS (P.R. Taylor), ABACUS (T. Helgaker, H.J. Aa. Jensen, P. Jørgensen, and J. Olsen), and ECP routines by A. V. Mitin and C. van Wüllen. For the Current Version. Available online: http://www.cfour.de (accessed on 11 December 2020).

84. Gauss, J.; Stanton, J.F. Analytic CCSD(T) Second Derivatives. *Chem. Phys. Lett.* **1997**, *276*, 70–77. [CrossRef]

85. Spackman, P.R.; Jayatilaka, D.; Karton, A. Basis Set Convergence of CCSD(T) Equilibrium Geometries Using a Large and Diverse Set of Molecular Structures. *J. Chem. Phys.* **2016**, *145*, 104101. [CrossRef]

86. Feller, D.; Peterson, K.A. Probing the Limits of Accuracy in Electronic Structure Calculations: Is Theory Capable of Results Uniformly Better Than "Chemical Accuracy"? *J. Chem. Phys.* **2007**, *126*, 114105. [CrossRef]

87. Wang, S.; Schaefer, H.F. The Small Planarization Barriers for the Amino Group in the Nucleic Acid Bases. *J. Chem. Phys.* **2006**, *124*, 044303. [CrossRef] [PubMed]

88. Bak, K.L.; Gauss, J.; Jørgensen, P.; Olsen, J.; Helgaker, T.; Stanton, J.F. The Accurate Determination of Molecular Equilibrium Structures. *J. Chem. Phys.* **2001**, *114*, 6548. [CrossRef]

89. Martin, J.M.L.; Taylor, P.R. Structure and Vibrations of Small Carbon Clusters from Coupled-Cluster Calculations. *J. Phys. Chem.* **1996**, *100*, 6047. [CrossRef]

90. Xie, Y.; Scuseria, G.E.; Yates, B.F.; Yamaguchi, Y.; Schaefer, H.F. Methylnitrene: Theoretical Predictions of its Molecular Structure and Comparison with the Conventional C-N Single Bond in Methylamine. *J. Am. Chem. Soc.* **1989**, *111*, 5181. [CrossRef]

91. Thimmakondu, V.S. The Equilibrium Geometries of Heptatriynylidene, Cyclohepta-1,2,3,4-tetraen-6-yne, and Heptahexaenyli-dene. *Comput. Theor. Chem.* **2016**, *1079*, 1–10. [CrossRef]

92. Thimmakondu, V.S.; Karton, A. Energetic and Spectroscopic Properties of the Low-Lying C_7H_2 Isomers: A High-Level Ab Initio Perspective. *Phys. Chem. Chem. Phys.* **2017**, *19*, 17685–17697. [CrossRef]

93. Thimmakondu, V.S.; Karton, A. The Quest for the Carbene Bent-Pentadiynylidene Isomer of C_5H_2. *Chem. Phys.* **2018**, *515*, 411–417. [CrossRef]

94. Thirumoorthy, K.; Viji, M.; Pandey, A.P.; Netke, T.G.; Sekar, B.; Yadav, G.; Deshpande, S.; Thimmakondu, V.S. Many Unknowns Below or Close to the Experimentally Known Cumulene Carbene—A Case Study of C_9H_2 Isomers. *Chem. Phys.* **2019**, *527*, 110496. [CrossRef]

95. Thimmakondu, V.S.; Ulusoy, I.; Wilson, A.K.; Karton, A. Theoretical Studies of Two Key Low-Lying Carbenes of C_5H_2 Missing in the Laboratory. *J. Phys. Chem. A* **2019**, *123*, 6618–6627. [CrossRef] [PubMed]

96. Thimmakondu, V.S. Molecules in Laboratory and in Interstellar Space? In Proceedings of the 71st International Symposium on Molecular Spectroscopy, Urbana, IL, USA, 20–24 June 2016; p. RH05.

97. Tsipis, A.C.; Depastas, I.G.; Tsipis, C.A. Diagnosis of the σ-, π-and (σ+ π)-Aromaticity by the Shape of the NICSzz-Scan Curves and Symmetry-Based Selection Rules. *Symmetry* **2010**, *2*, 284–319. [CrossRef]

98. Furukawa, S.; Fujita, M.; Kanatomi, Y.; Minoura, M.; Hatanaka, M.; Morokuma, K.; Ishimura, K.; Saito, M. Double Aromaticity Arising From σ- and π-Rings. *Commun. Chem.* **2018**, *1*, 60. [CrossRef]

99. Kalita, A.J.; Rohman, S.S.; Kashyap, C.; Ullah, S.S.; Guha, A.K. Double Aromaticity in a $BBe_6H_6^+$ Cluster with A Planar Hexacoordinate Boron Structure. *Chem. Commun.* **2020**, *56*, 12597–12599. [CrossRef] [PubMed]

100. Lee, T.J.; Taylor, P.R. A Diagnostic for Determining the Quality of Single-Reference Electron Correlation Methods. *Int. J. Quantum Chem.* **1989**, *36*, 199–207. [CrossRef]

101. Petrie, S.; Herbst, E. Some Interstellar Reactions Involving Electrons and Neutral Species: Attachment and Isomerization. *Astrophys. J.* **1997**, *491*, 210–215. [CrossRef]

102. Zhang, Y.; Xu, X.; Goddard, W.A. Doubly Hybrid Density Functional for Accurate Descriptions of Nonbond Interactions, Thermochemistry, and Thermochemical Kinetics. *Proc. Natl. Acad. Sci. USA* **2009**, *106*, 4963–4968. [CrossRef]
103. Zhang, I.Y.; Wu, J.; Xu, X. Extending the Reliability and Applicability of B3LYP. *Chem. Commun.* **2010**, *46*, 3057–3070. [CrossRef]
104. Grimme, S. Semiempirical Hybrid Density Functional with Perturbative Second-Order Correlation. *J. Chem. Phys.* **2006**, *124*, 034108. [CrossRef]
105. Grimme, S.; Neese, F. Double-Hybrid Density Functional Theory for Excited Electronic States of Molecules. *J. Chem. Phys.* **2007**, *127*, 154116. [CrossRef] [PubMed]
106. Beyer, T.; Swinehart, D.F. Algorithm 448: Number of Multiply-Restricted Partitions. *Commun. ACM* **1973**, *16*, 379. [CrossRef]